Quantitative analysis by in vivo imaging of the dynamics of vascular and axonal networks in injured mouse spinal cord

Cyril Dray, Geneviève Rougon[1], and Franck Debarbieux

Unité Mixte de Recherche 6216, Centre National de la Recherche Scientifique, Université de la Méditerranée, Institut de Biologie du Développement de Marseille-Luminy, Case 907, Parc Scientifique de Luminy, 13288 Marseille Cedex 9, France

Edited by Lynn T. Landmesser, Case Western Reserve University, Cleveland, OH, and approved April 10, 2009 (received for review January 8, 2009)

Understanding the endogenous repair capacity of spinal cord is pivotal to develop strategies to improve it. Here we design a paradigm of spinal cord lesion in the dorsal column using a 2-photon microscopy technique to dynamically and chronically monitor simultaneous changes of vascular and axonal networks in living mice up to 4 months postinjury. High-resolution images showed that early explorative sprouting of surviving injured axons resulted in extensive regrowth until and past the lesion site within 2 months. Blood vessel density was transiently up-regulated and most neurovascular interactions occurred within 2 weeks. Time-lapse analysis showed that neovessels exerted a potent growth stimulating action, but no guidance effect on neighboring sprouts, possibly because of their geometry and plasticity. Nevertheless, if reconnection depends on axon sprout density, stimulation of angiogenesis would probably be beneficial to repair. More generally, this imaging approach is showing promise to aid in monitoring brain diseases and the efficacy of potential treatments.

angiogenesis | axon regeneration | in vivo 2-photon imaging | spinal cord injury | time lapse

Spinal cord injury (SCI) induces dramatic cellular and molecular changes in the neuronal environment resulting overall in impaired axonal regeneration (1–3). Posttraumatic disturbance of blood perfusion is, for example, responsible for secondary damage (3), and reports suggest that stimulation of posttraumatic angiogenesis with vascular endothelial growth factor (VEGF) improves functional recovery of injured rodents (4, 5). Optimizing treatments to target vascularization might then be a valuable therapeutic strategy in the context of SCI, but the finding that VEGF signals on axons in addition to blood vessels (6) challenges the importance of the vascular response in the recovery process.

The conclusion of these studies is that the dynamics of the interactions occurring between axons and blood vessels and the influence of vascularization on axon regrowth have to be characterized thoroughly at the single axon level. Investigative tools are scarce, however, and poorly compatible with the determination of kinetics as most of the acquired knowledge comes from histological studies on spinal cord sections sampled from different subjects at different time points. A pioneering in vivo study combining wide-field imaging and the use of transgenic mice with fluorescent spinal cord axons reported observations of individual axons over 1 week after SCI (7). However, only a few axons were sampled per mouse and they were observed for a limited time. We sought to design a more dedicated imaging protocol on the basis of 2-photon microscopy (8, 9) to resolve populations of injured axons in 3 dimensions (3D) in the same mouse and to optimize the method to allow dynamic studies over a period of several months. Dual-color imaging allowed simultaneous visualization of posttraumatic vascular responses and for the first time neurovascular interactions were characterized in vivo at a cellular level.

Our data confirm the existence of an endogenous repair program where central branches of dorsal root ganglion (DRG) axons have the intrinsic capacity to regenerate. Analysis at different time points of identified individual axons revealed an 8-fold acceleration of axon growth in the vicinity of blood vessels. However biphasic and dynamic remodeling of blood vessels limited neurovascular interactions mainly to the first 2 weeks postinjury.

Results

Non Invasiveness of Repeated Imaging Sessions. We first established surgery and imaging protocols allowing successive imaging sessions with no sign of damage or impairment to axonal and vascular networks. We verified that performing surgery (opening without lesion) repeatedly on the same mouse at least 3 times at 2- to 5-day intervals ($n = 6$ mice) did not induce significant axon losses or changes in blood vessel patterns (Fig. 1*A*). Moreover, we verified that the partial absence of bone protection over 2 vertebrae was not responsible for secondary lesions at least for a period of 2 months. Our quantification method for axons and blood vessels (Fig. 1*B*) revealed a good stability over time (Fig. 1*C*). Our experimental protocol was thus validated for addressing the question of the dynamics of neuronal and vascular changes following spinal cord lesion (Fig. 1 *B* and *D* and supporting information (*SI*) Movie S1). Therefore a lesion paradigm producing a limited astrocyte activation characterized by a local overexpression of chondroitin sulfate proteoglycan NG2 (Fig. S1) but no noticeable change in glial fibrillary acidic protein (GFAP) (Fig. 1*E* and Fig. S2) was designed to study neurovascular interactions in the presence of focal scar environment (10).

Axonal Degeneration and Regeneration After a Minimal Pin Lesion. In every mouse, we characterized the temporal and spatial fate of a population of ≈40 fluorescent green axons that had been severed by pin lesion of the dorsal column (Fig. 2*A*). This population was imaged before the lesion, 20 min postlesion and some days or weeks after the lesion. Twenty minutes after injury, half of the axons had degenerated acutely at the lesion epicenter (53% ± 6.4%, $n = 8$ mice) as indicated by the presence of retraction bulbs. This acute degeneration (AD) was responsible for a retraction of at least 35.38 μm (±3.38, $n = 8$ mice) and was

Author contributions: G.R. and F.D. designed research; C.D. and F.D. performed research; F.D. contributed new reagents/analytic tools; C.D. and F.D. analyzed data; and G.R. and F.D. wrote the paper.

The authors declare no conflict of interest.

This article is a PNAS Direct Submission.

Freely available online through the PNAS open access option.

[1]To whom correspondence should be addressed. E-mail: rougon@ibdml.univ-mrs.fr.

This article contains supporting information online at www.pnas.org/cgi/content/full/0900222106/DCSupplemental.

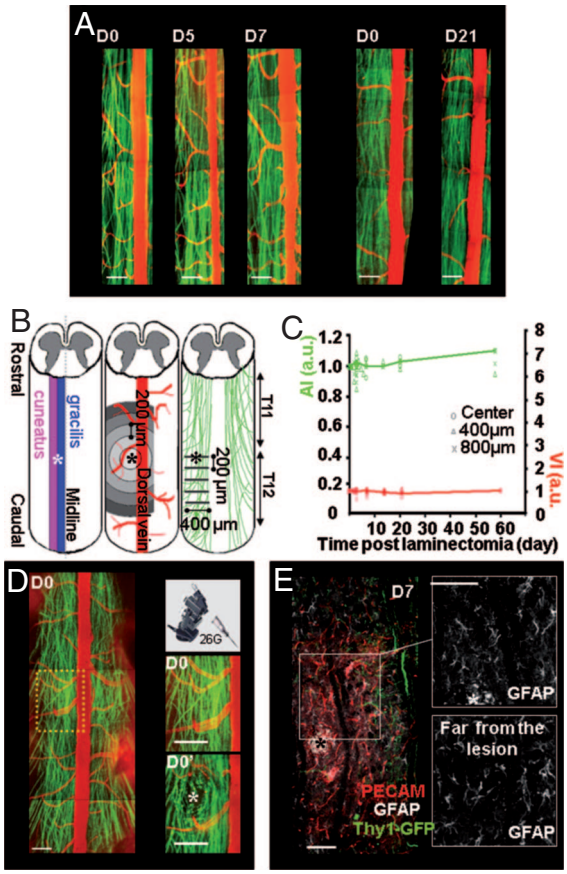

Fig. 1. Noninvasive in vivo imaging protocol and spinal cord lesion model. (*A*) Dorsal spinal cord images of 2 Thy1-GFP sham mice operated on D0 and reopened either on D5 and D7, or on D21, illustrate the stability of vascular (red) and axonal (green) networks. (*B*) Lesion (*) was applied in the dorsal column at the border between *gracilis* and *cuneatus* fasciculi; vessel density was quantified in concentric areas around the lesion epicenter in the acquired field of view; axon density was quantified in 200 μm spaced successive planes caudally to the lesion. (*C*) Axon index (AI, green) and vessel index (VI, red) were stable in space and time for sham-operated mice ($n = 6$). Average evolutions are plotted. (*D*) Initial field of view and zooms of the lesion site before (D0) and after (D0′) superficial pin insertion. Retraction bulbs formed on severed axons (Movie S1). (*E*) Horizontal spinal cord section immunostained against PECAM (vessels, red) and glial fibrillary acidic protein (GFAP, astrocytes, white; GFP axons, green) 7 days after lesion. The shape of astrocytes and the intensity of GFAP staining did not differ in area near or far from the lesion epicenter (Fig. 1). (Scale bars: *A–D*, 200 μm; *E*, 50 μm.)

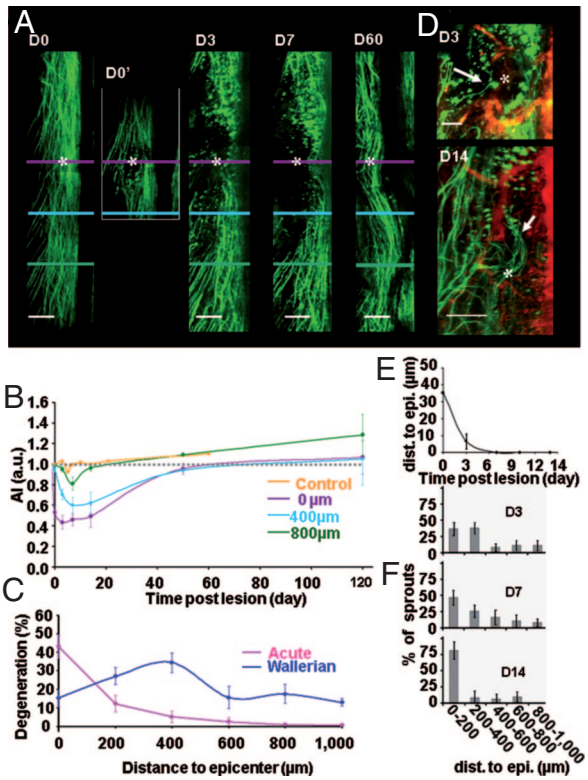

Fig. 2. Time course of degeneration and regeneration of DRG axons. (*A*) The same population of axons was repeatedly imaged before (D0), immediately after (D0′), on D3, D7, and D60 after lesion. Acute degeneration on D0′ was followed by progressive Wallerian degeneration. Lesion site (*) was fully recolonized by axons on D60. (*B*) Evolution of average axon index (AI) at various distances from the lesion plane (violet) ($3 \leq n \leq 8$). (*C*) Spatial extent of acute and maximal Wallerian degeneration. (*D*) Two cases of axon sprouts (→) reaching the lesion site on D3 or growing through the lesion site on D14 (→). (*E*) Evolution of the shortest distance between severed axon tips and lesion epicenter ($n = 8$). (*F*) Spatial distribution of axon sprouts as a function of time. (Scale bars: *A*, 200 μm; *D*, 100 μm.)

mainly localized in the first 200 μm around the epicenter (Fig. 2 *B* and *C*).

In agreement with an earlier report (7), this phase of AD was followed by a phase of secondary Wallerian degeneration (WD). WD was progressive over at least 1 week and responsible for the progressive reduction of axon number at various distances from the lesion site (Fig. 2 *B* and *E*). Axon losses because of WD were already obvious 400 μm away from the epicenter on day 3 postinjury (D3), but they were significant 800 μm away only by the end of the first week. The area concerned with WD was at least 5 times larger than AD and WD was responsible for a loss of 10% of the axons ($\pm$4.3%, $n = 7$) 1,000 μm away from the epicenter on D7 (Fig. 2*C*). At the lesion site, 23% ($\pm$5%, $n = 8$, $P = 0.016$) of the axons which showed no discontinuities or blebblings, and were considered as anatomically uninjured immediately after the lesion underwent WD in the following week.

Despite on-going WD, one-third of the damaged axons (33% $\pm$ 4.67, $n = 8$ mice, 296 axons) already exhibited sprouts from their proximal endings on D3 (Fig. 2*D*). A given parent axon often presented multiple sprouting branches, typically 1.57 per axon ($\pm$0.14, $n = 296$ axons) mainly located ($\approx$80%) in the first 400 μm from the lesion epicenter (Fig. 2*F*). Interestingly, at least 1 of these sprouts had reached the lesion plane as early as D3 in 6 of 8 mice (Fig. 2*D*). The proportion of sprouts reaching the lesion site increased with time (Fig. 2*F*) and by D14 many sprouts had grown through and passed the lesion (Fig. 2*D*). Regrowth until or at the lesion site was complete and stable at 2 (Fig. 2*A*) and 4 months after injury as indicated by axon indexes (AI) (AI = 107% $\pm$ 16%, $n = 3$ and AI = 120% $\pm$ 15%, $n = 2$, respectively) (Fig. 2*B*). Regenerated axons even exited the lesion site to progressively reinvade location as distal as 400 μm away from the epicenter where AI recovered from 47% $\pm$ 20% on D7 to 80% $\pm$ 11% after 2 months ($n = 3$, $P = 0.04$).

Vascular Response to the Lesion. The lesion also produced localized destruction of blood vessels and hence disruption of the blood supply. This was soon compensated for by a phase of spontaneous angiogenesis which was obvious on D3 and maximal by D7 (Fig. 3*A–C*). Numerous new vessel branches with small ($\approx$6 μm) and medium ($\approx$30 μm) diameters appeared in and around the lesion site (Tables S1 and S2). Although vessel density appeared globally increased in the whole area observed, the highest increase was found in the first 400 μm surrounding the lesion

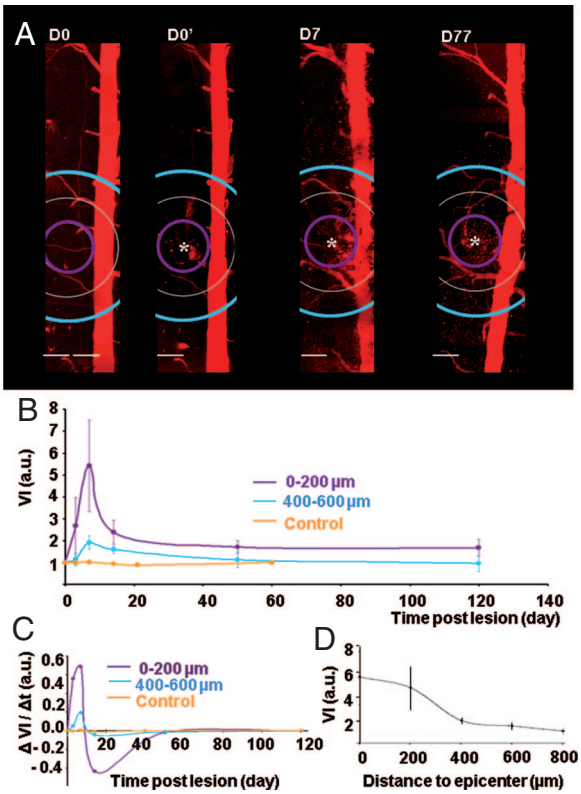

Fig. 3. Time course of changes in the vascular network. (*A*) Vascularization of the dorsal spinal cord imaged before (D0), immediately after (D0′), and on D7 and D77 after lesion. (*B*) Evolution of average vessel index (VI) at various distances from the lesion site (*) ($2 \leq n \leq 10$, Tables S1 and S2). (*C*) Average speed of vascular changes as a function of time. Negative values correspond to down-regulation of angiogenesis. (*D*) Spatial extent of vascular changes ($n = 6$). (Scale bar, 200 μm.)

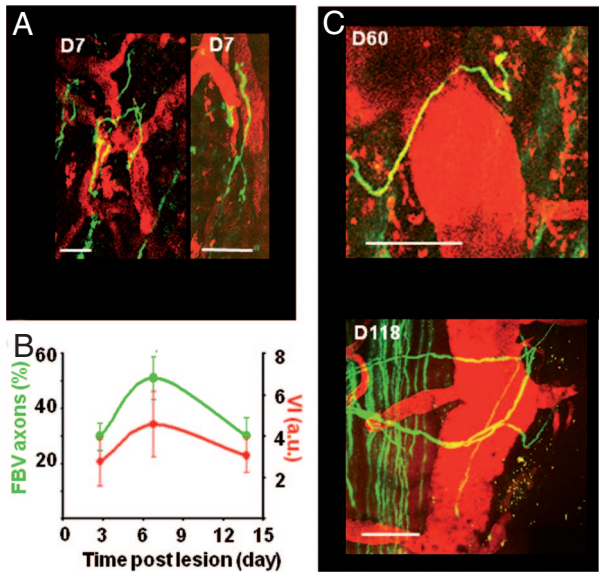

Fig. 4. Vascular scaffold for axon growth. (*A*) Examples of sprouts growing along newly formed blood vessels on D7 ($n = 171$). (*B*) Percentage of axons following blood vessels (FBV axons, green) as a function of time and corresponding evolution of vessel density (VI, red). (*C*) Examples of sprouts growing along the dorsal vein at D60 or D118 after lesion. (Scale bar, 50 μm.)

epicenter (Fig. 3*D*). This resulted in a 540% (±210%, $n = 7$, $P = 0.03$) increase of the vessel index (VI) (see *Methods*; Fig. 3*B*).

A fast pruning and remodeling of vessels took place in the second week, leaving only a few stable vessel branches directed to the lesion (Fig. 3 *A* and *C*). The large negative changes of VI between D7 and D14 confirmed that the local vascular network was very plastic and strongly remodeled during the second week. Blood irrigation of the lesion was only slightly enhanced over the long term (VI = 1.66 ± 0.25, $n = 3$ at 200 μm on D50) (Fig. 3 *A* and *B*).

Neurovascular Interaction. We assessed interactions between vessels and regrowing axons during the first 2 weeks postinjury. In this time window, many axon sprouts grew in close vicinity to newly formed blood vessels with tortuous trajectories, differing from the privileged axial orientation of DRG axons (Figs. 4 and 5*G*). The percentage of sprouts following blood vessels (FBV) increased from 29% (±5.2%, $n = 171$) on D3 to 53% (±8.5%, $n = 171$, $P = 0.04$) on D7 and decreased back to 30% (±6.9%, $n = 70$, $P = 0.04$) on D14, directly matching the evolution of VI (Fig. 4*B*). Such spatial distribution of axons reflected their clear preference for blood vessel versus parenchyma (Fig. S3). Moreover, we observed some axons growing on dorsal vein surfaces after SCI (4 of 9 mice) (Fig. 4*C*), a feature never observed in noninjured animals and supporting the idea of a sustained trophic effect of blood vessels on regrowing axons.

We tested whether this affinity for blood vessels could influence axon growth by analyzing the dynamics of individual sprouts that were clearly identifiable from one imaging session to the next. Although variable, elongation of FBV sprouts between D3 and D7 (143 μm ± 73.4 μm, $n = 6$) was enhanced almost 8-fold (**, $P = 0.008$) compared to elongation of non-FVB (N-FBV) sprouts (18.4 μm ± 13.10 μm, $n = 6$) (Fig. 5 *A* and *B*). Fast growth of axons along vessel walls was confirmed by in vivo time lapse experiments on D6 to −8. Although the speed of elongation was irregular over time with periods of sprout stagnation or even regression (Fig. 5*D*), we recorded velocities as high as 80 μm/h close to blood vessels and an average velocity of 17 μm/h over 6 h (Fig. 5 *C* and *D* and Movie S2, Movie S3, and Movie S4).

Spinal cord rewiring could fully benefit from accelerated axon growth if blood vessels could also guide elongation toward the lesion. We did indeed find cases where vessels helped the sprouts to develop toward or around the lesion. But we also observed cases where the sprouts were extensively growing on blood vessels in a direction opposite to the lesion (Fig. 5*E*). Quantification revealed that the same proportion of FBV and N-FBV sprouts was directed toward the lesion (FBV: 66.9% ± 6.87, $n = 78$; N-FBV: 61.50% ± 8.9%, $n = 85$) (Fig. 5*F*). Moreover long-non direct or looping trajectories were repeatedly observed at the surface of vascular branches (Fig. 5*G* and Movie S5). Together these observations indicate that vessels do not guide axons toward their targets.

Dynamic and Selective Sprout Elimination. Irrespective of their growth rate many sprouts failed to contribute to the final reinvasion of the lesion site. Regenerative sprouting appeared as a dynamic explorative process where some axon branches underwent selective elimination while other new branches extended in different directions off the same parent axon (Fig. 6*A* and Movie S3). Elimination sometimes occurred by progressive retraction over several days (Fig. 6*A*) whereas in some cases elimination occurred by a rapid degenerative process lasting only a few hours (Fig. 6*B*). In all cases however, new axonal extensions appeared in the same time window and in the same environment as sprout degeneration (Fig. 6*C*) or sprout retraction (Movie S3). Such observations ruled out a global nonsupportive effect of the environment as an explanation for sprout elimination.

NEUROSCIENCE

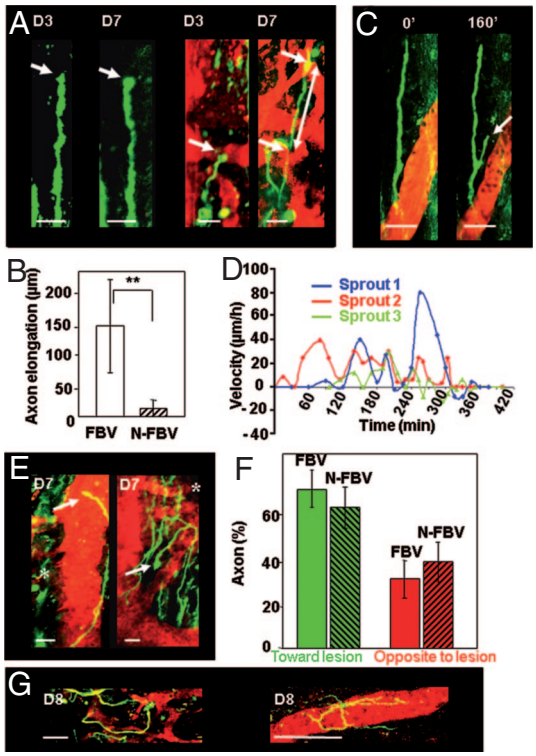

Fig. 5. Trophic effect of vessels on axons but lack of guidance to the lesion. (*A*) Absence of elongation between D3 and D7 for a sprout growing >50 μm from vessels (*Left*) compared to extensive elongation (125 μm, white arrows) for another sprout growing along vessels (*Right*). (*B*) Average elongation between D3 and D7 for FBV ($n = 6$) and non-FBV (N-FBV, $n = 6$) sprouts. (*C*) Fast development of a side branch (arrow) at the surface of the closest blood vessel while its parent sprout did not grow (3-h time lapse on D8). (*D*) Fluctuations of velocities for 3 FBV sprouts (3 different colors) in 3 mice on D8. (*E*) On D7, a FBV sprout (→) had grown past the lesion site (*) whereas another FBV sprout (→) had developed in the opposite direction. (*F*) FBV population of sprouts ($n = 78$) is not significantly biased toward the lesion compared to the N-FBV population ($n = 85$). (*G*) Examples of looping and inefficient elongations of FBV sprouts on D8. (Movie S2, Movie S3, Movie S4) (Scale bars: *A*, 25 μm; *C* and *G*, 50 μm.)

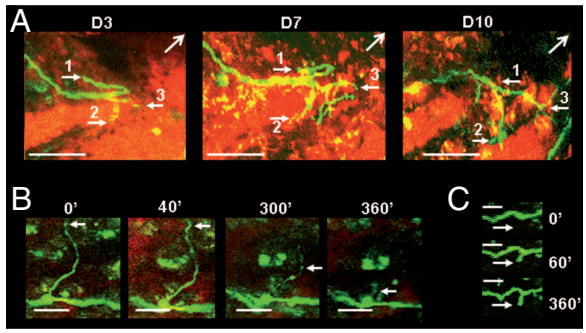

Fig. 6. Dynamic sprouting and pruning of axons. (*A*) Repeated observations of an identified severed axon on D4, D7, and D10. One branch retracted (sprout 1), another branch was stable (sprout 2), and a third one developed into several sprouts (sprout 3). Lesion epicenter was outside the field of view in the direction of (→). (*B*) Degeneration of a long sprout branch during a 6-h time lapse on D8. (*C*) Meanwhile a neighboring axon initiated elongation in the same traumatic environment. (Scale bars: *A*, 50 μm; *B* and *C*, 20 μm.)

Discussion

We have developed a dedicated noninvasive in vivo imaging protocol to follow the dynamics of degeneration/regeneration in populations of injured spinal cord axons while simultaneously monitoring the fate of the vascular network in the same animal. Repeated imaging sessions provided a unique way to differentiate surviving axons from regenerating axons, a problem encountered in earlier studies (11–13). We have demonstrated that growth kinetics of sensory regenerating axons are strongly enhanced by their vicinity to posttraumatic angiogenic vessels after SCI but that vessels do not help axons to recover their initial trajectories. These in vivo observations provide dynamic and 3D spatial extensions to immunostaining works (14–16) where endothelial markers were used to assess angiogenic responses regardless of the vessels' functional relevance.

The optical properties of the tissue limited our penetration depth to the first 200 μm in spinal cord dorsal column where vascularization was modest in control conditions (17). It was strongly up-regulated by the lesion and thus appears to be a good model to study neurovascular interactions without interference of a glial scar (13) whose formation was reduced by our strategy of a minimally invasive lesion.

We show that severed central branches of DRG axons have the unexpected endogenous ability to regenerate over at least several millimeters in the spinal cord, despite the current belief that only their peripheral branches can spontaneously regenerate in the absence of a preconditioning peripheral lesion (18, 19) or pharmacological treatment (20–22). Supporting our data is a report of successful axonal regeneration of grafted DRG neurons in rat spinal cord (13), although that study could not exclude modifications of the extracellular environment by cografted satellite cells. Axons, however, showed different susceptibility and/or responses to the traumatic environment (13) as supported by the imaging of sprouting at the lesion site already at D3, when WD was still ongoing in neighboring axons whose resistance to postlesion ischemic (3), excitotoxic (23), or inflammatory insults (24) (Fig. S4) was probably weaker.

Although the fate of every severed fluorescent axon could not be assessed individually over time because of difficulties of identification when dealing with large populations of axons, several lines of evidence support their regenerative behavior. First, axon segments that reinvaded the lesion site were fluorescent and hence probably had a DRG phenotype (7, 25). Second, as early as D3, sprouting was observed on the proximal end of severed axons. In addition, as expected from progressive regeneration of axons by sprouting, the front of these sprouts was progressively shifted toward the lesion over the first 2 weeks with some sprouts clearly extending through and past the lesion epicenter over several hundreds of micrometers. Third, after 2 and 4 months, the number of axons counted along the traumatized area and hundreds of micrometers distally to the lesion was similar to the number before injury with no evidence of the neuronal circuit being reorganized to bypass the lesion (26).

We found that regenerating axons tend to grow in close contact with blood vessels, which provide them with a fast-track and nutritionally favorable environment. This affinity persisted beyond the peak of the angiogenic response and could also involve preexisting vessels such as the dorsal vein. The interaction resulted in a strong enhancement of sprout dynamics and a surprising elongation velocity for axons (up to 80 μm/h). Our in vivo time lapse experiments fully highlighted this phenomenon, which is otherwise minimized by averaging extremely irregular kinetics. At the peak of the angiogenic response the axon elongation velocity was on average 8 times larger than reported in the first few days posttrauma (7). Better oxygenation and increased metabolism might explain part of this effect given that the oxygen content usually falls by 50% at 20 μm away from vessel walls (27). Axon elongation might also benefit from the scaffold formed by the vascular network whose extracellular matrix can offer an anchoring and growth-promoting substrate.

The vascular environment is enriched in components such as laminin (15) (Fig. S5) and collagen (28), which are lacking in the brain parenchyma. Finally, we cannot rule out the possible release from vessels of yet unidentified trophic factors for axons.

Despite this strong influence of an angiogenic response on axonal regeneration, various factors seemed to limit its beneficial impact on spinal cord repair. Elongating axons were not guided to the lesion. This could be because of the geometry of the vessel network as its orientation is mostly perpendicular to the dorsal column axis and to the high plasticity of vascular branches. Indeed, axons had to bypass vascular obstacles that were formed continuously or elongate on top of randomly remodeling substrates; such features represent constraints incompatible with a straight trajectory.

Some axons nevertheless benefitted from vascular support to accelerate their growth toward the lesion. This support was only transient and was limited mainly to an early and narrow time window representing less than 20% of the time required for complete recolonization of the lesion site. Moreover if vessels act as a source of neurotrophic factors for axons (6), their disappearance might lead to elimination of active axonal sprouts (29). In our model, the strong down-regulation of vessel density was not explained by cystic cavern formation (15, 16) and is more consistent with a programmed sequence of events involving endogenous antiangiogenic factors (30).

If reconnection of regenerating axons with their dedicated targets proceeds from random encounter events it follows that maintenance of a high density of active sprouts should increase the probability of productive interactions. This might be achieved by stabilization and consolidation of neovessels in the long term by manipulating posttraumatic angiogenesis (31). Visualization of axon–blood vessel interactions will undoubtedly be instrumental for assessing future potential treatments.

Methods

Animal Surgery. Twenty-four adult transgenic Thy1GFP-M mice (25) were used in this study (sham $n = 7$; injured $n = 17$). Animals were deeply anesthetized with Ketamine-Xylasine mixture (100 mg/kg; 10 mg/kg) supplemented hourly. Laminectomia was carried out at the thoracic T11–T13 level after fixation on a modified Cunningham spinal cord holder. Dura mater was kept intact. One hundred to 200 μL of Rhodamin B isothiocyanate-Dextran solution (70 kDa Sigma; 20 mg/mL in PBS) were injected into the tail vein before imaging. Animals were freely breathing and kept warm at 36°C during imaging. After imaging, the spinal cord surface was protected by a thick layer of agarose and the skin was sutured. A similar protocol was successfully repeated up to 6 times on the same mouse over a 4-month period, at various times postinjury (ex: D3 stands for 3 days post-injury). This surgery produced no damage to vascular and neuronal networks in sham-operated mice (Fig. 1 *A* and *C*).

Spinal Cord Lesion. A $26G^{3/8}$ needle was placed at the border between the *gracile* and the *cuneate fasciculi* of 1 exposed dorsal horn using a micropositioner (WPI) (Fig. 1 *B* and *D*). A blade was slowly inserted to a depth of 500 μm and immediately withdrawn. All procedures were approved by the National Animal Studies Committee of France (authorization no. 13,300).

In Vivo Imaging. A femtosecond pulsed infrared laser (Mai-Tai, Spectra-Physics) tuned at 850 nm was coupled to a Zeiss 2-photon microscope (Axioskop 2FS LSM 510) modified to position the stereotactic apparatus below the water immersion 20× objective (NA = 1.0). GFP (500–550 nm) or Rhodamin (575–640 nm) signals were simultaneously detected on 2 nondescanned detectors. ImageJ free software was used to process image stacks. ImageJ 3D Stitching macro, ''pcm3d,'' was kindly provided by Stephan Preibisch (University of Leipzig, Germany).

Analysis. Maximal or average projections of stitched stacks are presented in the figures. Analysis and quantification were done manually from raw 3D stacks with the assistance of self-written imageJ macros. The lesion site was carefully relocated on image stacks at every time point thanks to readily observable spatial cues. Concentric circles whose radii were incremented by steps of 200 μm were centered on the lesion epicenter and superimposed on image stacks (Fig. 1*B*). For each area defined by 2 successive circles, the surface covered by blood vessels was evaluated and expressed as the percentage of its value before injury. These values are termed ''vessel index'' (VI). Positive changes of VI indicated new vessel formation and negative changes, vessel pruning, and reorganization. Every 200 μm caudally to the lesion, we determined the number of axon branches intercepting virtual planes perpendicular to the spinal cord axis (Fig. 1*B*). Each number was then divided by the number of axons initially counted at the same location before injury to define a local ''axon index'' (AI). Axon branches were considered as sprouts if thinner than parent axons and terminated by a typical axon tip. Sprouts were classified as either following a blood vessel (FBV) if their end tip was less than 5 μm away from a vessel wall and nonfollowing blood vessel (N-FBV) if the distance exceeded 5 μm. Sprouts were defined as growing opposite to the lesion if their terminal end pointed in a direction more than 90° away from the expected longitudinal direction of growth. Sprouts were otherwise considered as growing toward the lesion.

Results were expressed as mean values ± SE and *P* value of 1-tailed Student's *t* test was calculated.

ACKNOWLEDGMENTS. We thank P. Weber for skillfull technical assistance. Our work was supported by grants to G.R. and F.D. from the Centre National de la Recherche Scientifique (CNRS), the Institut de Recherche pour la Moelle Epinière (IRME), the Délégation aux Entreprises (DGE), and Pôle de Compétitivité ORPHEME (project MEDUL) and by a doctoral fellowship from Région/CNRS to C.D. Imaging was performed on the cellular imaging platform of the Luminy site (PICsiL).

1. Gurtner GC, Werner S, Barrandon Y, Longaker MT (2008) Wound repair and regeneration. *Nature* 453:314–321.
2. Coleman M (2005) Axon degeneration mechanisms: Commonality amid diversity. *Nat Rev Neurosci* 6:889–898.
3. Mautes AE, Weinzierl MR, Donovan F, Noble LJ (2000) Vascular events after spinal cord injury: Contribution to secondary pathogenesis. *Phys Ther* 80:673–687.
4. Facchiano F, *et al.* (2002) Promotion of regeneration of corticospinal tract axons in rats with recombinant vascular endothelial growth factor alone and combined with adenovirus coding for this factor. *J Neurosurg* 97:161–168.
5. Widenfalk J, *et al.* (2003) Vascular endothelial growth factor improves functional outcome and decreases secondary degeneration in experimental spinal cord contusion injury. *Neuroscience* 120:951–960.
6. Carmeliet P, Tessier-Lavigne M (2005) Common mechanisms of nerve and blood vessel wiring. *Nature* 436:193–200.
7. Kerschensteiner M, Schwab ME, Lichtman JW, Misgeld T (2005) In vivo imaging of axonal degeneration and regeneration in the injured spinal cord. *Nat Med* 11:572–577.
8. Davalos D, *et al.* (2008) Stable in vivo imaging of densely populated glia, axons and blood vessels in the mouse spinal cord using two-photon microscopy. *J Neurosci Methods* 169:1–7.
9. Helmchen F, Denk W (2005) Deep tissue two-photon microscopy. *Nat Methods* 2:932–940.
10. Busch SA, Silver J (2007) The role of extracellular matrix in CNS regeneration. *Curr Opin Neurobiol* 17:120–127.
11. Cafferty WB, McGee AW, Strittmatter SM (2008) Axonal growth therapeutics: Regeneration or sprouting or plasticity? *Trends Neurosci* 31:215–220.
12. Steward O, Zheng B, Tessier-Lavigne M (2003) False resurrections: Distinguishing regenerated from spared axons in the injured central nervous system. *J Comp Neurol* 459:1–8.
13. Davies SJ, *et al.* (1997) Regeneration of adult axons in white matter tracts of the central nervous system. *Nature* 390:680–683.
14. Benton RL, Maddie MA, Minnillo DR, Hagg T, Whittemore SR (2008) Griffonia simplicifolia isolectin B4 identifies a specific subpopulation of angiogenic blood vessels following contusive spinal cord injury in the adult mouse. *J Comp Neurol* 507:1031–1052.
15. Loy DN, *et al.* (2002) Temporal progression of angiogenesis and basal lamina deposition after contusive spinal cord injury in the adult rat. *J Comp Neurol* 445:308–324.
16. Imperato Kalmar EL, McKinney RA, Schnell L, Rubin BP, Schwab ME (1997) Local changes in vascular architecture following partial spinal cord lesion in the rat. *Exp Neurol* 145:322–328.
17. Koyanagi I, Tator CH, Peter L (1993) Three-dimensional analysis of the vascular system in the rat spinal cord with scanning electron microscopy of vascular corrosion casts. Part 1: Normal spinal cord. *Neurosurgery* 33:277–283.
18. Neumann S, Bradke F, Tessier-Lavigne M, Basbaum AI (2002) Regeneration of sensory axons within the injured spinal cord induced by intraganglionic cAMP elevation. *Neuron* 34:885–893.
19. Qiu J, *et al.* (2002) Spinal axon regeneration induced by elevation of cyclic AMP. *Neuron* 34:895–903.
20. Wang R, *et al.* (2008) Persistent restoration of sensory function by immediate or delayed systemic artemin after dorsal root injury. *Nat Neurosci* 11:488–496.
21. Ramer MS, Priestley JV, McMahon SB (2000) Functional regeneration of sensory axons into the adult spinal cord. *Nature* 403:312–316.
22. Neumann S, Woolf CJ (1999) Regeneration of dorsal column fibers into and beyond the lesion site following adult spinal cord injury. *Neuron* 23:83–91.

23. Park E, Velumian AA, Fehlings MG (2004) The role of excitotoxicity in secondary mechanisms of spinal cord injury: A review with an emphasis on the implications for white matter degeneration. *J Neurotrauma* 21:754–774.
24. Fitch MT, Doller C, Combs CK, Landreth GE, Silver J (1999) Cellular and molecular mechanisms of glial scarring and progressive cavitation: In vivo and in vitro analysis of inflammation-induced secondary injury after CNS trauma. *J Neurosci* 19:8182–8198.
25. Feng G, *et al.* (2000) Imaging neuronal subsets in transgenic mice expressing multiple spectral variants of GFP. *Neuron* 28:41–51.
26. Bareyre F, Kerschensteiner M, Misgeld T, Sanes JR (2004) The injured spinal cord spontaneously forms a new intraspinal circuit in adult rats. *Nat Neurosci* 7:269–277.
27. Tsai AG, Johnson PC, Intaglietta M (2003) Oxygen gradients in the microcirculation. *Physiol Rev* 83:933–963.
28. Okada M, *et al.* (2007) Expression and role of type I collagen in a rat spinal cord contusion injury model. *Neurosci Res* 58:371–377.
29. Wang H, Tessier-Lavigne M (1999) En passant neurotrophic action of an intermediate axonal target in the developing mammalian CNS. *Nature* 401:765–769.
30. Mueller CA, Conrad S, Schluesener HJ, Pietsch T, Schwab JM (2007) Spinal cord injury-induced expression of the antiangiogenic endostatin/collagen XVIII in areas of vascular remodeling. *J Neurosurg Spine* 7:205–214.
31. Ferrara N, Kerbel RS (2005) Angiogenesis as a therapeutic target. *Nature* 438:967–974.